9-22-2016

Imaging population transfer in atoms with ultrafast electron pulses

Hua-Chieh Shao
Purdue University, hshao@unl.edu

Anthony F. Starace
University of Nebraska-Lincoln, astarace1@unl.edu

PHYSICAL REVIEW A **94**, 030702(R) (2016)

Imaging population transfer in atoms with ultrafast electron pulses

Hua-Chieh Shao[1] and Anthony F. Starace[2]
[1]*Department of Physics and Astronomy, Purdue University, West Lafayette, Indiana 47907, USA*
[2]*Department of Physics and Astronomy, University of Nebraska, Lincoln, Nebraska 68588-0299, USA*
(Received 7 April 2016; published 22 September 2016)

We propose the use of ultrafast electron diffraction (UED) to image a controllable, laser-driven coherent electron population transfer in lithium atoms with currently available femtosecond electron pulses. Our simulations demonstrate the ability of ultrafast electrons to image such an electronic population transfer, thus validating UED as a direct means of investigating electron dynamics. Provided the incident electron pulses have sufficient temporal resolution, the diffraction images are shown to resolve also the relative phases of the target electronic wave functions.

DOI: 10.1103/PhysRevA.94.030702

To understand various reaction mechanisms in gas-phase or condensed materials, one requires knowledge of electronic and nuclear motions and the interplay among these degrees of freedom during the reactions. Ultrafast electron diffraction (UED) and microscopy provide subangstrom spatial and femtosecond temporal resolutions that allow the direct imaging of the *atomic* motions [1–4]. For example, structural evolutions during phase transitions have been mapped using ultrafast electron microscopy and crystallography [5–7]. Also, diffraction images have identified transient molecular structures [8] and established evidence of deformation and dissociation of molecules interacting with laser pulses [9]. Nowadays, electron pulses with femtosecond (fs) durations have been reported [10–14]. Recently, single-electron pulses with a full width at half maximum (FWHM) duration of 28 fs have been demonstrated [15]. Various schemes for further compression of these pulses to attosecond durations [16–20] and for reaching attosecond resolution by optical gating [21] have been proposed. Simulations of various electron scattering processes employing attosecond duration incident electron pulses, whether treated simply as potential scattering processes [22] or more rigorously as coherent scattering processes [23–25], have demonstrated the ability of such ultrashort electron pulses to image electronic motions in target atoms and molecules.

Current electron pulse durations, however, are still insufficient to resolve the electronic motions, with typical durations $\lesssim 1$ fs, in most gas-phase reactions. Moreover, while the importance of the longitudinal coherence of the electron pulses for imaging electronic motions has been recognized [24,25], the necessary precision for characterizing and controlling the coherence of electron pulses is still experimentally challenging [26], and theoretical modeling of the various degrees of coherence in simulations is difficult. In order to flexibly overcome these difficulties, a time-varying electronic system whose characteristic time scale is longer than existing electron pulse durations would be useful. For such a system, one could investigate how the properties of the incident electron pulses affect their diffraction patterns, examine the sensitivity of electron pulses to the electronic movements, and obtain information for developing experimental techniques for producing and employing attosecond electron pulses. Hence, we investigate here the imaging of picosecond (ps) time-scale coherent electronic motion in atoms by UED. Specifically, we probe laser-driven electron population transfer in lithium atoms with femtosecond electron pulses, as shown schematically in Fig. 1.

The electronic motion we investigate is adiabatic passage of the lithium atom's valence electron from the $2s$ state to the $2p$ state by a frequency-chirped laser pulse. We have chosen this electron population transfer process because it has been experimentally demonstrated in alkali-metal atoms [27–29] and because of its simplicity, controllability, and robustness [29,30]. The underlying mechanism can be understood from a dressed-state picture. In the presence of a periodic laser field, the atomic levels are lifted or lowered owing to the dressing of the laser photons. The population transfer process starts from a large negative laser detuning so that the diabatic energy of the one-photon dressed $2s$ state is far below that of the $2p$ state of the lithium atom. Then the frequency of the laser is swept upward (red to blue), so that the diabatic energy of the dressed $2s$ state crosses that of the $2p$ state. However, the adiabatic energies have an avoided crossing connecting the dressed $2s$ and $2p$ states at large negative and positive detunings. Therefore, if the frequency of the laser pulse is varied slowly, then the electronic state adiabatically follows the evolution and, accordingly, the entire $2s$ population can be transferred to the $2p$ state.

The laser-induced population transfer from the $2s$ to the $2p$ state of the lithium atom is shown in Fig. 2. The temporal envelope and the time-dependent frequency of the linearly chirped laser pulse are shown as a function of time in Fig. 2(a), while the populations of the $2s$, $2p$, and $3d$ states of Li are shown as functions of time in Fig. 2(b). The laser field is assumed to be linearly polarized along the z axis with a peak intensity of 1.93×10^7 W/cm^2, and its Gaussian envelope has a duration (FWHM) of 2.0 ps. The instantaneous frequency equals the $2s$-$2p$ resonant frequency at the peak of the laser pulse at a time ≈ 3.63 ps after the turn on of the pulse. One sees that almost 100% of the $2s$ state population is transferred to the $2p$ state, while the population in the $3d$ excited state is negligibly small throughout the entire process. The time scale of the adiabatic passage is regulated by the period of Rabi oscillation, where the Rabi frequency of a two-state system in a monochromatic laser field is defined by $\Omega = \boldsymbol{d} \cdot \boldsymbol{E}/\hbar$, where $\boldsymbol{d}$ is the transition dipole moment between the states, and $\boldsymbol{E}$ is the laser electric field. Therefore, the time scale of the adiabatic passage can be controlled by the intensity and the rate of chirp of the laser pulse. For the laser profiles shown here, the time

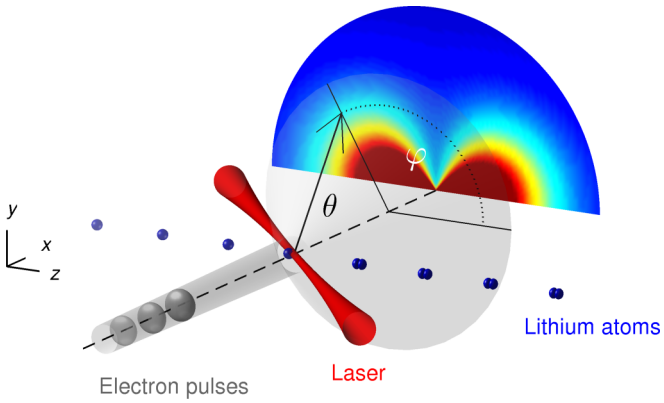

FIG. 1. Schematic setup for time-resolved UED from lithium atoms undergoing laser-driven electron population transfer. The valence electrons of the lithium atoms are adiabatically transferred from the $2s$ to the $2p$ states through a level crossing induced by the frequency-swept laser pulse. This time-varying electronic motion in the lithium atoms is probed by an ultrafast electron pulse at certain delay times and a detector records the diffraction pattern of the scattered electron pulse. For future reference, we define here the coordinate system and the scattering angles θ and φ.

scale of the population transfer is about 3.0 ps, which is much longer than the duration of current state-of-the-art ultrafast electron pulses.

The averaged valence electron densities in the yz plane (cf. Fig. 1) are shown as inset figures in Fig. 2(b) at delay times $t_d = 1.0$, 3.0, 4.0, and 6.0 ps (relative to the turn on of the laser pulse). They are calculated from the $2s$ and $2p$ densities weighted by their populations at the given delay

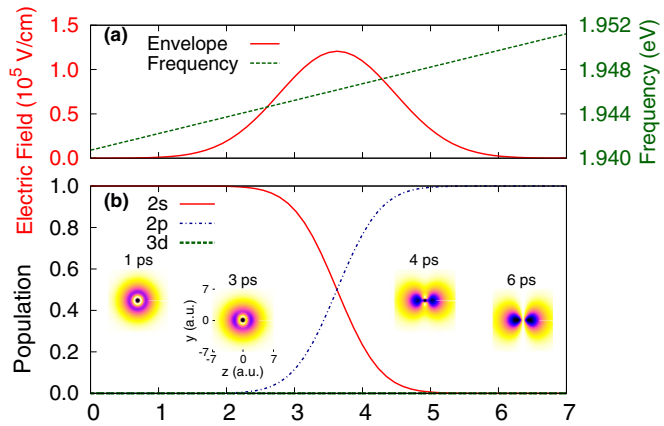

FIG. 2. (a) Envelope (left ordinate) and instantaneous frequency (right ordinate) of the chirped laser pulse used to transfer population from the $2s$ state to the $2p$ state of the lithium atom. The linearly polarized laser pulse is assumed to have a Gaussian envelope with a 2.0 ps duration (FWHM) and a peak electric field amplitude of 1.21×10^5 V/cm. (b) Time-dependent populations of the $2s$, $2p$, and $3d$ states of the lithium atom induced by the laser pulse in (a). The insets illustrate the changing symmetry of the valence electron charge density in the yz plane (cf. Fig. 1) as a function of increasing delay time for $t_d = 1.0$, 3.0, 4.0, and 6.0 ps. The spatial extent of the electron density at $t_d = 3.0$ ps (cf. inset) is shown explicitly in atomic units (a.u.) of length (1 a.u. = 0.529 Å).

times. One can clearly see the change of the symmetry and nodal structure of these weighted electron densities during the population transfer. At $t_d = 1.0$ ps an isotropic density with a single nodal circle signifies the character of the $2s$ orbital. As the $2p$ population grows, the symmetry changes to the dumbbell shape of the $2p$ state and the nodal circle disappears.

At particular delay times t_d during the adiabatic population transfer we calculated the ensemble-averaged differential probability for an incident electron to be scattered into a solid angle about the angles θ and φ (cf. Fig. 1), where the ensemble average is over the transverse positions (i.e., the impact parameters) of the lithium atoms in the atomic beam (for details, see the Supplemental Material [31]). The electron pulses are assumed to have a Gaussian distribution of 100 fs duration (FWHM) with a kinetic energy of 10 keV in the laboratory frame. The electron pulse's angular divergence is $\pm 10^{-4}$ rad. We assume that the lithium atoms are moving so slowly in comparison to the electron pulse that they may be treated as stationary in the laboratory frame. Spatial inhomogeneities such as those originating from the group velocity mismatch between the laser and electron pulses are not included in our simulations because experimental techniques have been developed to mitigate such effects [2]. We thus assume that each incident electron pulse "sees" a homogeneous ensemble of lithium atoms of 50 μm thickness having a density of 10^{10} cm^{-3} [32]. The Li atoms are projected onto a plane perpendicular to the direction of the incident electrons. We calculate the scattering probabilities for the incident electron pulses from the Li atoms in this plane. The simulations are performed in the center-of-mass frame, although the diffraction images change only very slightly in the laboratory frame because of the heavy mass of the lithium atoms and the high energy of the electron pulses. Only the $1s$, $2s$, and $2p$ states are used to calculate the scattering amplitudes since the populations of other excited states are negligible. Since the kinetic energies of the scattered electrons are not usually measured in diffraction experiments, inelastic transitions must be considered when calculating the diffraction images. In our simulations the transitions to final states of lithium atoms having principal quantum numbers less than ten and orbital angular momenta less than nine are included.

The diffraction images for 100-fs electron pulses at delay times $t_d = 1.0$, 3.7, and 6.0 ps during the $2s$-to-$2p$ population transfer in the lithium atom targets are shown in Fig. 3(a). One observes a dramatic increase of the scattering intensity in the forward direction as the delay time increases, which reflects the sensitivity of electron pulses to the population transfer in the lithium atoms. This strong enhancement in the forward direction occurs because the $2p$ state has a much larger scattering probability than the $2s$ state and because inelastic scattering transitions are usually peaked in the forward direction [24,40]. Note that the population transfer here is a coherent process; it thus provides a system for studying the effects of the incident electron pulse coherence on the diffraction images. Specifically, our expectation is that the interference contrast of a diffraction image is sensitive to the longitudinal and transverse coherences of the incident electron beam (cf. Secs. 6 and 7 of Ref. [26]).

In order to compare the effects of pulse duration on the diffraction patterns, we show in Figs. 3(b)–3(d) our calculated

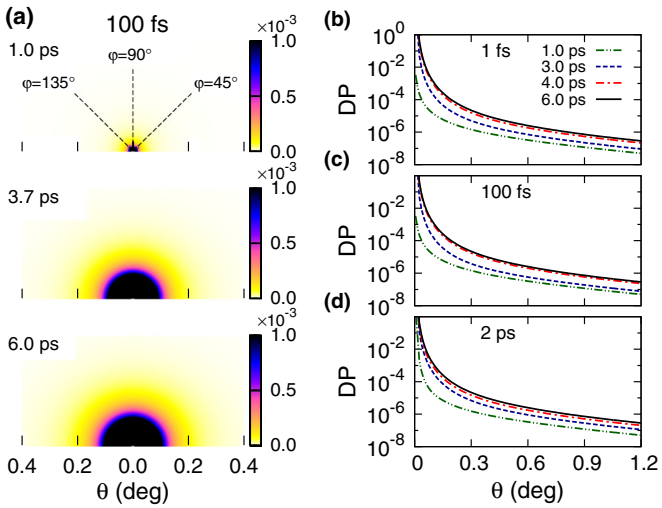

FIG. 3. (a) Ensemble-averaged differential probabilities (DPs) for 100-fs ultrafast electron pulses scattered from lithium atoms (undergoing laser-driven population transfer) at delay times $t_d = 1.0$, 3.7, and 6.0 ps. The kinetic energy of the electron pulse is 10 keV in the laboratory frame. See Fig. 1 for definitions of the scattering angles θ and φ. Only the upper half scattering images are shown (owing to symmetry). (b)–(d) DPs for (b) 1 fs, (c) 100 fs, and (d) 2 ps electron pulses as functions of the scattering angle θ, for $\varphi = 0°$, at delay times $t_d = 1.0$, 3.0, 4.0, and 6.0 ps.

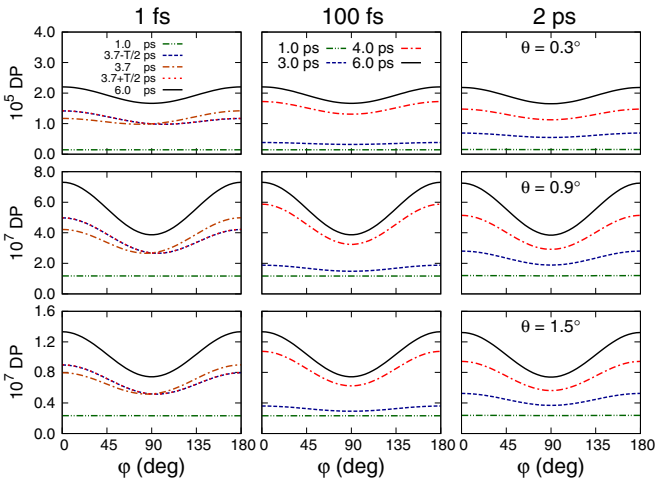

FIG. 4. The ensemble-averaged DPs for 1-fs (left column), 100-fs (middle column), and 2-ps (right column) pulses scattered from the time-dependent $2s$-to-$2p$ population transfer in the lithium atoms as functions of the azimuthal scattering angle φ at the scattering angles $\theta = 0.3°$ (top row), 0.9° (middle row), and 1.5° (bottom row) (cf. Fig. 1). Different curves correspond to different pump-probe delay times, indicated by the legends. The delay times for the 1-fs pulse differ from those for the 100-fs and 2-ps pulses in order to illustrate the ability of the 1-fs electron pulses to resolve the asymmetric electronic motion oscillating with the beat period ($T = 2.13$ fs) of the $2s$ and $2p$ states. Note also that the 1-fs differential probabilities for $t_d = (3.7 - T/2)$ and $(3.7 + T/2)$ ps are indistinguishable on the scale of the figure.

results for the ensemble-averaged differential probabilities (DPs) for 1-fs, 100-fs, and 2-ps electron pulses as functions of the scattering angle θ. The azimuthal scattering angle is $\varphi = 0°$. The corresponding bandwidths (FWHM) of these electron pulses are about 1.8, 1.8×10^{-2}, and 9.1×10^{-4} eV, respectively. One observes that in each case the differential probabilities increase as the time delay increases, reflecting the fact that the $2p$ state has a larger scattering probability than the $2s$ state. However, the 2-ps case differs in its angular and temporal behaviors compared to those for the 1- and 100-fs pulses. First, the differential probability for the 2-ps case already has a larger peak at $\theta = 0°$ when $t_d = 1.0$ ps. Second, since the $2p$ population increases from 11.5% to 76.8% as the time delay increases from $t_d = 3.0$ to 4.0 ps [cf. Fig. 2(b)], the changes of the differential probabilities for the 1- and 100-fs pulses reflect such rapid growth between those two time delays. For the 2-ps pulse, owing to its long duration, the increase of the differential probability with increasing time delay is more uniform at large scattering angles ($\theta > 0.3°$), thus failing to reflect the rapid increase of the $2p$ population between those two delay times. However, the similarities in the results for the 1- and 100-fs pulses indicate that, provided the electron pulses have adequate temporal resolution, their small pulse bandwidths (with respect to their large kinetic energy) result in electron pulses that are essentially monoenergetic. Hence, the diffraction patterns are insensitive to the details of the pulse shape and directly reflect the target structures.

The electron pulses we consider are not only sensitive to the temporal variations of the target electron state populations, but are also able to differentiate the symmetry of the electronic state during the population transfer. In order to demonstrate this, the DPs for the three pulse durations as functions of azimuthal scattering angle φ at different pump-probe delay times are shown in Fig. 4 for three scattering angles $\theta = 0.3°$, 0.9°, and 1.5°. The results in the three columns correspond to those for the three pulse durations, while the results in the three rows correspond to the three scattering angles θ denoted in the last column. The pump-probe delay times for the 1-fs pulse differ from those for the 100-fs and 2-ps pulses in order to show that the 1-fs pulse is able to resolve the asymmetric diffraction patterns with respect to $\varphi = 90°$ for differences in the time delays comparable to the beat period $T = 2.13$ fs of the $2s$ and $2p$ states. The 100-fs and 2-ps pulses are unable to resolve the 2.13-fs beating of the $2s$ and $2p$ states during the population transfer. For all pulse durations, the symmetries of the diffraction patterns change from an isotropic distribution of the DP (i.e., independent of φ) at $t_d = 1.0$ ps to a dumbbell symmetry at $t_d = 6.0$ ps, consistent with the $2s$-to-$2p$ population transfer. Moreover, for any scattering angle θ, the DPs at the delay times $t_d = 1.0$ and 6.0 ps are almost identical for all pulse durations, whereas differences in the DPs appear between $t_d = 1.0$ and 6.0 ps. [Note that the φ dependence of the scattering patterns shown in Fig. 4 cannot be easily seen in Fig. 3(a) owing to the order-of-magnitude larger scattering probabilities in the forward direction.]

In order to illustrate the capability of UED to measure the time-dependent $2s$-to-$2p$ electron population transfer in the Li atom, we have fit the DPs at the delay times $t_d = 3.0$, 3.7, and 4.0 ps to a linear combination of those at $t_d = 1.0$ and 6.0 ps, which respectively represent the DPs for the $2s$ and $2p$ states. The results for the $2s$ population at the given delay times are

TABLE I. Retrieval of the time-dependent $2s$ population during the laser-driven $2s$-to-$2p$ population transfer in Li atoms using the UED scattering patterns. The $2s$ populations at delay times $t_d = 3.0$, 3.7, and 4.0 ps are extracted by a least-squares fitting of the DPs of the 100-fs and 2-ps pulses at each pulse duration and scattering angle θ to a linear combination of the DPs at delay times $t_d = 1.0$ and 6.0 ps, which are essentially those for the $2s$ and $2p$ states, respectively. These fitting results are compared with the $2s$ populations predicted by the simulation whose results are shown in Fig. 2(b) and given in the last column.

Delay time (ps)	Fitting		Simulation
	100 fs	2 ps	
3.0	88.5%	73.5%	88.5%
3.7	44.1%	46.7%	44.1%
4.0	23.3%	34.9%	23.2%

shown in Table I for pulse durations of 100 fs and 2 ps. Results for the scattering angles $\theta = 0.3^\circ$, 0.9°, and 1.5° all render the same $2s$ population at a given t_d. The 100-fs pulse precisely retrieves the $2s$ population predicted by our simulation [shown in Fig. 2(b)], while the $2s$ population obtained by our fitting procedure for the 2-ps pulse differs significantly, thus showing its insufficient temporal resolution.

The results in Table I show that the 100-fs pulse can accurately determine the time-dependent populations of the $2s$ and $2p$ states. To obtain more complete information on the electronic motion on the time scale of the beat period, a shorter electron pulse duration is required, as shown in Fig. 4 for the 1-fs electron pulse. One observes in Fig. 4 asymmetric diffraction patterns with respect to $\varphi = 90^\circ$ at three delay times that differ by half the beat period, centered at $t_d = 3.7$ ps. Since opposite parities are involved in the beat oscillation, an asymmetric wiggling motion of the target electron is faithfully imaged by the ultrafast electrons. Moreover, the essentially identical diffraction patterns at $t_d = 3.7 - T/2$ and $3.7 + T/2$ ps show that the asymmetry of the diffraction pattern oscillates with the beat period. Note that these rapid asymmetric changes in the diffraction patterns cannot be obtained by modeling UED as potential scattering from the target charge densities [24,41], since in that approximation the elastic scattering differential cross sections are always centrosymmetric according to Friedel's law [42].

In conclusion, we have demonstrated the imaging of the laser-driven electron population transfer in lithium atoms by UED. The simulations show how the pulse duration affects the level of information on the electronic motions that can be extracted from the diffraction patterns. In particular, if the durations of the electron pulses are shorter than the $2s$-$2p$ beat period, then the diffraction images show asymmetric angular distributions. Since the conventional interpretation [43] of electron diffraction cannot model the asymmetry, it must be modified to properly interpret experimental results once electron pulses have sufficient temporal resolution [24]. Finally, we note that a similarly motivated proposed experiment for observing electronic motion has recently been made in the field of x-ray scattering: Suominen and Kirrander [44] propose the creation of a coherent superposition of Rydberg states in rare-gas atoms whose electronic motion would be slow enough to observe with current state-of-the-art ultrashort x-ray pulses.

We thank Herman Batelaan and Martin Centurion for their critical reading of our manuscript. This work was supported in part by the U.S. Department of Energy, Office of Science, Basic Energy Sciences, under Award No. DE-SC0012193 (H.-C. S.) and by the U.S. National Science Foundation under Grant No. PHYS-1505492 (A.F.S.). This work was completed utilizing the facilities of the Holland Computing Center at the University of Nebraska.

[1] A. H. Zewail, Four-dimensional electron microscopy, Science **328**, 187 (2010).

[2] G. Sciaini and R. J. D. Miller, Femtosecond electron diffraction: Heralding the era of atomically resolved dynamics, Rep. Prog. Phys. **74**, 096101 (2011).

[3] R. J. D. Miller, Femtosecond crystallography with ultrabright electrons and x-rays: Capturing chemistry in action, Science **343**, 1108 (2014).

[4] J. M. Thomas, R. K. Leary, A. S. Eggeman, and P. A. Midgley, The rapidly changing face of electron microscopy, Chem. Phys. Lett. **631-632**, 103 (2015).

[5] H. Kleinschmidt, A. Ziegler, G. H. Campbell, J. D. Colvin, and O. Bostanjoglo, Phase transformation analysis in titanium at nanosecond time resolution, J. Appl. Phys. **98**, 054313 (2005).

[6] M. Gao *et al.*, Mapping molecular motions leading to charge delocalization with ultrabright electrons, Nature (London) **496**, 343 (2013).

[7] B.-K. Yoo, O.-H. Kwon, H. Liu, J. Tang, and A. H. Zewail, Observing in space and time the ephemeral nucleation of liquid-to-crystal phase transitions, Nat. Commun. **6**, 8639 (2015).

[8] H. Ihee, V. A. Lobastov, U. M. Gomez, B. M. Goodson, R. Srinivasan, C.-Y. Ruan, and A. H. Zewail, Direct imaging of transient molecular structures with ultrafast diffraction, Science **291**, 458 (2001).

[9] J. Yang, J. Beck, C. J. Uiterwaal, and M. Centurion, Imaging of alignment and structural changes of carbon disulfide molecules using ultrafast electron diffraction, Nat. Commun. **6**, 8172 (2015).

[10] M. Aidelsburger, F. O. Kirchner, F. Krausz, and P. Baum, Single-electron pulses for ultrafast diffraction, Proc. Natl. Acad. Sci. USA **107**, 19714 (2010).

[11] J. Hoffrogge, J. P. Stein, M. Krüger, M. Förster, J. Hammer, D. Ehberger, P. Baum, and P. Hommelhoff, Tip-based source of femtosecond electron pulses at 30 keV, J. Appl. Phys. **115**, 094506 (2014).

[12] L. Waldecker, R. Bertoni, and R. Ernstorfer, Compact femtosecond electron diffractometer with 100 keV electron bunches approaching the single-electron pulse duration limit, J. Appl. Phys. **117**, 044903 (2015).

[13] C. Gerbig, A. Senftleben, S. Morgenstern, C. Sarpe, and T. Baumert, Spatio-temporal resolution studies on a highly compact ultrafast electron diffractometer, New J. Phys. **17**, 043050 (2015).

[14] P. Zhu *et al.*, Femtosecond time-resolved MeV electron diffraction, New J. Phys. **17**, 063004 (2015).

[15] A. Gliserin, M. Walbran, F. Krausz, P. Baum, Sub-phonon-period compression of electron pulses for atomic diffraction, Nat. Commum. **6**, 8723 (2015).

[16] E. Fill, L. Veisz, A. Apolonski, and F. Krausz, Sub-fs electron pulses for ultrafast electron diffraction, New J. Phys. **8**, 272 (2006).

[17] P. Baum, and A. H. Zewail, Attosecond electron pulses for 4D diffraction and microscopy, Proc. Natl. Acad. Sci. USA **104**, 18409 (2007).

[18] S. A. Hilbert, C. Uiterwaal, B. Barwick, H. Batelaan, and A. H. Zewail, Temporal lenses for attosecond and femtosecond electron pulses, Proc. Natl. Acad. Sci. USA **106**, 10558 (2009).

[19] A. Gliserin, A. Apolonski, F. Krausz, and P. Baum, Compression of single-electron pulses with a microwave cavity, New J. Phys. **14**, 073055 (2012).

[20] P. Hansen, C. Baumgarten, H. Batelaan, and M. Centurion, Dispersion Compensation for Attosecond Electron Pulses, Appl. Phys. Lett. **101**, 083501 (2012).

[21] M. Kozák, J. McNeur, K. J. Leedle, N. Schönenberger, A. Ruehl, I. Hartl, J. S. Harris, R. L. Byer, and P. Hommelhoff, Optical gating and streaking of free-electrons with attosecond precision, arXiv:1512.04394.

[22] H.-C. Shao and A. F. Starace, Detecting Electron Motion in Atoms and Molecules, Phys. Rev. Lett. **105**, 263201 (2010).

[23] H.-C. Shao and A. F. Starace, Time-resolved ultrafast electron $(e,2e)$ momentum spectroscopy, Phys. Rev. A **87**, 050701(R) (2013).

[24] H.-C. Shao and A. F. Starace, Imaging coherent electronic motion in atoms by ultrafast electron diffraction, Phys. Rev. A **88**, 062711 (2013).

[25] H.-C. Shao and A. F. Starace, Imaging electronic motions in atoms by energy-resolved ultrafast electron diffraction, Phys. Rev. A **90**, 032710 (2014).

[26] P. Baum, On the physics of ultrashort single-electron pulses for time-resolved microscopy and diffraction, Chem. Phys. **423**, 55 (2013).

[27] B. Broers, H. B. van Linden van den Heuvell, and L. D. Noordam, Efficient Population Transfer in a Three-Level Ladder System by Frequency-swept Ultrashort Laser Pulses, Phys. Rev. Lett. **69**, 2062 (1992).

[28] P. Balling, D. J. Maas, and L. D. Noordam, Interference in climbing a quantum ladder system with frequency-chirped laser pulses, Phys. Rev. A **50**, 4276 (1994).

[29] J. S. Melinger, S. R. Gandhi, A. Hariharan, D. Goswami, and W. S. Warren, Adiabatic population transfer with frequency-swept laser pulses, J. Chem. Phys. **101**, 6439 (1994).

[30] N. V. Vitanov, T. Halfmann, B. W. Shore, and K. Bergmann, Laser-induced population transfer by adiabatic passage techniques, Annu. Rev. Phys. Chem. **52**, 763 (2001).

[31] See Supplemental Material at http://link.aps.org/supplemental/10.1103/PhysRevA.94.030702, which includes Refs. [33–39], for details of our simulations of the laser-driven population transfer in the Li atom and of the ultrafast electron diffraction from that time-dependent electron transfer process.

[32] J. Gillot, A. Gauguet, M. Büchner, and J. Vigué, Optical pumping of a lithium atomic beam for atom interferometry, Eur. Phys. J. D **67**, 263 (2013).

[33] R. G. Newton, *Scattering Theory of Waves and Particles* (McGraw-Hill, New York, 1966).

[34] H. A. Bethe and R. W. Jackiw, *Intermediate Quantum Mechanics*, 2nd ed. (W. A. Benjamin, New York, 1968).

[35] F. Herman and S. Skillman, *Atomic Structure Calculations* (Prentice-Hall, Englewood Cliffs, NJ, 1963).

[36] B. M. Smirnov, *Reference Data on Atomic Physics and Atomic Processes* (Springer, Berlin, 2008).

[37] W. I. McAlexander, E. R. I. Abraham, and R. G. Hulet, Radiative lifetime of the $2P$ state of lithium, Phys. Rev. A **54**, R5 (1996).

[38] M. E. Peskin and D. V. Schroeder, *An Introduction to Quantum Field Theory* (Addison-Wesley, Reading, MA, 1995).

[39] F. Ehlotzky, A. Jaroń, and J. Z. Kamiński, Electron-atom collisions in a laser field, Phys. Rep. **297**, 63 (1998).

[40] R. A. Bonham and M. Fink, *High Energy Electron Scattering* (Van Nostrand Reinhold, New York, 1974).

[41] G. Dixit, O. Vendrell, and R. Santra, Imaging electronic quantum motion with light, Proc. Natl. Acad. Sci. USA **109**, 11636 (2012).

[42] G. Friedel, Sur les symétries cristallines que peut révéler la diffraction des rayons Röntgen, C. R. Acad. Sci. **157**, 1533 (1913).

[43] J. C. H. Spence, Diffractive (lensless) imaging, in *Science of Microscopy*, edited by P. W. Hawkes and J. C. H. Spence (Springer, New York, 2007), Vol. II, p. 1196.

[44] H. J. Suominen and A. Kirrander, How to Observe Coherent Electron Dynamics Directly, Phys. Rev. Lett. **112**, 043002 (2014); see also the related comment [45] and the authors' reply [46].

[45] R. Santra, G. Dixit, and J. M. Slowik, Comment on "How to Observe Coherent Electron Dynamics Directly", Phys. Rev. Lett. **113**, 189301 (2014).

[46] H. J. Suominen and A. Kirrander, Authors' Reply, Phys. Rev. Lett. **113**, 189302 (2014).